

Influence of internal printing pattern and infill on morphological and dimensional properties of gluten-free bread manufactured by 3D printing

Carmen Molina-Montero, Adrian Matas, Marta Igual, Javier Martínez-Monzó,
Purificación García-Segovia ^{*}

i-Food Group, IIA-FoodUPV, Universitat Politècnica de València, Camino de Vera s/n, 46022, Valencia, España

ARTICLE INFO

Keywords:
Gluten-free bread
Pattern
Infill percentage
Crumb structure

ABSTRACT

The design and control of the internal structure in food 3D printing is a critical factor that determines the final properties and quality of food products. This study investigated the influence of internal structure design parameters in gluten-free bread made by 3D printing, specifically evaluating two patterns (rectilinear and concentric) and four infill percentages (30 %, 40 %, 50 %, and 60 %). The rheological properties of the dough, dimensional changes during printing and baking, colorimetric characteristics, and crumb structure were analyzed. The results showed that the dough presented a predominantly elastic behavior suitable for 3D printing. The rectilinear pattern exhibited higher dimensional stability during printing, while the concentric pattern showed higher moisture losses and, consequently lower dimensional deformations during baking. Analysis of the crumb structure revealed that the concentric pattern produced higher total porosity than the rectilinear pattern, with a more irregular pore distribution. Color differences were more pronounced in samples with 60 % infill, particularly in the rectilinear pattern. The results suggest that the selection of the pattern and percentage of infill should be based on the specific requirements of the final product.

1. Introduction

The technological revolution in the food industry has given rise to new and innovative production methods that are transforming the way food is manufactured and customised. Among these emerging technologies, 3D food printing, also known as Additive Manufacturing (AM), stands out as a technology that could have a major impact on the future of the food industry (Mantihal et al., 2020; Waseem et al., 2024). 3D food printing is a process based on the controlled deposition of layers of food material, which are overlapped on top of each other to build three-dimensional structures predefined by a digital model (Demei et al., 2022; Derossi et al., 2020). This technology not only makes it possible to adapt the design and morphology of foods but also to modify their functional characteristics. It can generate highly complex geometries and structures, which are difficult to achieve using traditional techniques (Zhang et al., 2022). Beyond its design capability, it allows the nutritional properties of foods to be tailored to meet specific dietary requirements while responding to the individual preferences or desires of consumers (Lin et al., 2020; Zhao et al., 2021).

The most widely used technique in 3D food printing is extrusion (Ma

and Zhang, 2022; Zhu et al., 2019), allowing the printing of food materials in a semi-solid or viscous state with Newtonian behaviour, which facilitates dispensing through the printing nozzle (Godoi et al., 2016; Voon et al., 2019). Given the complexity of food composition and physical properties, it is essential to characterise the food inks that will be subjected to the printing process (Feng et al., 2019; Godoi et al., 2016; Kim et al., 2018a). While the existing literature has mainly focused on the optimisation and development of printable inks, addressing aspects such as rheology, extrudability and compatibility with printing systems (Kim et al. 2018b; Tejada-Ortigoza and Cuan-Urquiza 2022; Bulut and Candogan 2022; Derossi et al. 2018), there are a limited number of studies related to the design and stability of the internal structure of the food (Chen et al., 2022; Nijdam et al., 2021; Zhao et al., 2021). Most of the studies related to the internal structure and how it affects the physical and mechanical properties of 3D printed objects come mainly from the areas of bioprinting and thermoplastics showing that the internal structure is crucial to maintain shape and avoid collapse (Decante et al., 2021; Fernandez-Vicente et al., 2016; Sood et al., 2010). This gap in knowledge about how the printing process influences the structural and microstructural properties of final food

* Corresponding author.

E-mail address: purgarse@tal.upv.es (P. García-Segovia).

products is particularly relevant, as understanding these aspects is fundamental to realise the full potential of this technology.

The internal structural design, including the pattern and percentage of infill, can have a significant impact on the textural properties and stability of the product, both after the printing process and after post-treatment (Liu and Zhang, 2021; Wang et al., 2024). The design of the internal structure in 3D printing not only provides the necessary structural support but also allows incorporating complexity into the design by allowing the design of internal networks with different density levels and geometric patterns, which influence the mechanical and textural characteristics of the food. The design can be controlled by multiple parameters in the slicer, but with the pattern and infill percentage being the two most important parameters affecting the internal structure (Liu, Bhandari, et al., 2018; Wang et al., 2024). The pattern defines the internal geometry of the structure, which can adopt various shapes such as rectilinear, honeycomb, and concentric, among others, while the infill percentage determines the density of the internal structure, which can vary between 1 % and 100 % (Liu, Bhandari, et al., 2018). The combination of these internal design parameters has a significant impact on the textural and mechanical properties of the final product. Some authors (Liu, Bhandari, et al., 2018; Liu and Zhang, 2021) have shown that the percentage of infill influences various aspects of the final printed product such as hardness, chewiness, or shape retention, although infill percentages above 50–60 % can lead to structural collapse of the shape. On the other hand, the pattern influences the hardness, weight, and porosity of the product (Caporizzi et al., 2018; Liu, Zhang, et al., 2018).

The importance of internal structural design becomes even more evident when considering post-processing processes, such as baking, drying, and freeze-drying, among others, where the internal configuration must maintain the structural integrity of the product while undergoing physicochemical transformations. Several researchers have studied how post-processing methods affect the morphological and dimensional properties of 3D-printed foods. In the case of cereal-based products, Severini et al. (2016) observed that structures with a higher percentage of infill showed better shape retention during baking, which is attributed to the fact that shape stability is highly correlated with the internal support structure of printed products. In terms of drying methods, Lille et al. (2018) compared conventional oven drying and freeze-drying on products with high fibre and protein content, finding that a more stable structure was obtained with an initial dry mass content of 35 % by freeze-drying. Liu & Zhang (2021) investigated the dimensional characteristics of different internal structures under different infill percentages and patterns, observing that percentages below 30 % resulted in structures unable to self-support, causing deformation. Although shrinkage may occur during post-processing due to moisture removal, the final products maintained their predefined dimensional characteristics well, possibly because the filling structure was not affected by the general shrinkage phenomenon. More recently, Pulatsu et al. (2022) developed combined 3D printing technologies to prevent collapse in biscuits during post-processing, demonstrating that different internal structures with 30 % and 50 % infill percentages and circular cubic and prismatic patterns maintained their shape without obvious collapse. These advances suggest the possibility of creating increasingly complex shapes that maintain their structural stability after printing, thus meeting future market demands.

3D printing is gaining increasing relevance in the bakery sector due to its ability to create complex structures and customized textures, particularly suited to meet the needs of gluten-free diets (Pradhan et al., 2024). However, printing wheat-based doughs is often hindered by the presence of gluten, which forms a highly elastic and cohesive network that complicates extrusion and shape fidelity. In contrast, gluten-free doughs, though lacking this natural viscoelastic network, can offer better control over extrusion behavior when optimized with binding agents, such as hydrocolloids, which help mimic gluten's structural function (Lisovska and Harasym, 2023).

Hydroxypropyl methylcellulose (HPMC), a hydrocolloid, and

psyllium, a soluble fiber with gelling properties, can improve the printability of gluten-free doughs. HPMC contributes to dough stability and gas retention by forming a thermally induced gel network during baking, enhancing crumb structure and bread volume. Psyllium reinforces dough elasticity and viscosity through its ability to form a weak gel matrix, facilitating extrusion. When combined, these ingredients allow for the formulation of gluten-free doughs with balanced viscoelastic properties, suitable for extrusion-based 3D printing (Mancebo et al., 2015; Manik and Nur, 2021; Torres-Pérez et al., 2024).

HPMC and psyllium also influence the internal structure of bread by promoting the formation, expansion, and stabilization of gas cells during fermentation and baking. The size, number, and distribution of these cells are key quality parameters in breadmaking (Relationship between instrumental parameters and sensory characteristics in gluten-free breads). In wheat bread, gluten forms a viscoelastic network capable of retaining gas, resulting in an open and elastic crumb (Rathnayake et al., 2018). In gluten-free bread, the absence of this protein network hinders gas retention and the formation of a honeycombed crumb, which usually results in denser and less aerated products. Therefore, functional ingredients such as HPMC and psyllium are essential not only for mechanical handling and printability but also for achieving a desirable internal morphology that mimics the aerated crumb typical of gluten-containing bread (Mancebo et al., 2015).

One of the major limitations in 3D food printing is the loss of structural integrity during post-processing, particularly in bakery products, where the expansion and evaporation of internal moisture during baking often lead to deformation of the printed geometry. This is especially critical in gluten-free formulations, which lack the viscoelastic gluten network that helps retain shape. The main objective of this study was to evaluate the effect of different internal structural design parameters on the 3D printing of gluten-free bread and their behaviour during post-processing. Specifically, the influence of two patterns (rectilinear and concentric) and four infill percentages (30 %, 40 %, 50 % and 60 %) on the structural stability and morphological properties of the products, both after printing and after the baking process, were analysed.

2. Materials and methods

2.1. Raw materials

The following ingredients were used for bread dough: gluten-free flour mix (Corn starch, rice flour, dextrose, vegetable fibers (psyllium and apple), stabilizer (HPMC), egg powder and salt) provided by Sinblat (Sinblat Alimentación Saludable S.L., Foios, Spain), baker's yeast supplied by Sosa Ingredients (Sosa Ingredients S.L.U., Barcelona, Spain), while salt, water, and oil were purchased from a local supermarket.

2.2. Preparation of bread dough

The bread dough formulation consisted of 41.52 % gluten-free flour, 56 % water, 0.88 % baker's yeast, 1.2 % oil, and 0.4 % salt (% w/w). Ingredients were mixed using a kneader (Kenwood chef classic, KM400/99 plus, Kenwood Corporation, Tokyo, Japan) at minimum speed for 45 s followed by 5 min at speed 2. The dough was fermented for 30 min. The resulting dough was then loaded into a syringe for the 3D printing process.

2.3. Rheology

The rheological characteristics of the bread dough were determined before the printing process using a Kinexus Pro+ rotational rheometer (Malvern Instruments, Worcestershire, UK) equipped with a parallel-plate geometry (40 mm diameter) and a gap of 1.0 mm. The linear viscoelastic region was determined through amplitude sweep tests with shear strain ranging from 0.1 % to 100 % at a constant frequency of 1 Hz.

Frequency sweep tests were conducted at a fixed stress of 1 Pa within a frequency range of 0.1–10 Hz. All measurements were performed in triplicate at 25 °C. Data acquisition and analysis were performed using rSpace software (Malvern Instruments, Worcestershire, UK).

2.4. 3D printing process

The 3D printing process was performed using a BCN 3D+ printer (BCN3D Technologies, Barcelona, Spain) fitted with a pasta extruder nozzle for food materials (BCN3D Technologies, Barcelona, Spain). The printer featured a syringe-pump extrusion mechanism and stepper motors for X-Y-Z axis positioning. A rectangular shape (70 × 30 × 20 mm) was designed using Tinkercad software (Autodesk, Inc., San Rafael, CA, USA) and sliced using Slic3r software (developed by Alessandro Ranelucci) to set the printing parameters. Two different infill patterns were studied: rectilinear and concentric (Fig. 1), each with four different infill densities (30 %, 40 %, 50 %, and 60 %). The printing parameters were set at an extrusion rate of 3 mL/min through a 1.2 mm diameter nozzle, with a nozzle speed of 20 mm/s and layer height of 1.2 mm. The process was carried out at room temperature, and the dough was printed directly onto a stainless-steel plate, which later served as the baking surface.

2.5. Post-Processing

The printed samples were baked in a convection oven (Convotherm Mini, Welbilt Iberia, Barcelona, Spain) at 190 °C for 22 min. After baking, samples were cooled to room temperature (25 °C) before analytical determinations.

Moisture loss was quantified by measuring the weight of the sample before and after post-treatment (baking) and was calculated using the following equation:

$$\text{Moisture loss (\%)} = \frac{W_p - W_b}{W_p} \times 100 \quad (1)$$

W_p : Weight Printed
 W_b : Weight Baked

2.6. Image analysis

2.6.1. Dimensional fidelity analysis of 3D printed and baked samples

Front and top-view images of each sample were captured

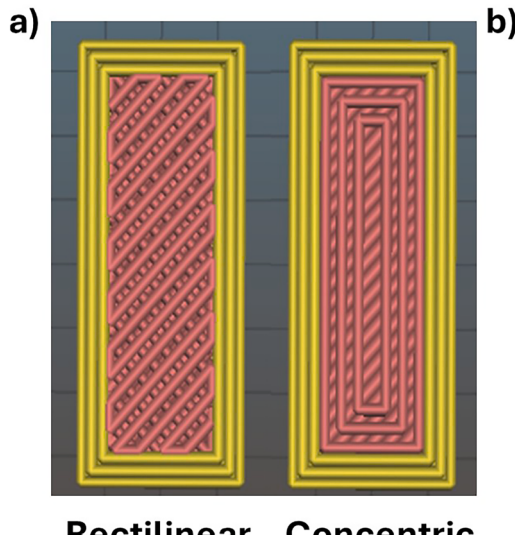


Fig. 1. Patterns used in 3D printing: a) rectilinear pattern and b) concentric pattern.

immediately after printing and after baking. Dimensional measurements were performed using ImageJ software (NIH, Washington, DC, USA). Length and width were measured from the top view, while height was measured from the front view (Molina-Montero et al. 2023).

2.6.2. Color analysis of dough, crust, and crumb

Color measurements were performed on digital images of the samples captured before (dough) and after baking (crust and crumb). The color analysis was conducted using ImageJ Software (NIH, Washington, DC, USA). RGB values were obtained from the digital images and subsequently converted to CIELAB color space parameters (L^* , a^* , b^*), where L^* represents lightness (0 = black, 100 = white), a^* indicates red (+) to green (-), and b^* indicates yellow (+) to blue (-). Chroma (C^*ab , saturation), and hue angle (h^*ab) were calculated. Color differences between samples were evaluated by comparing the pattern ($\Delta E-1$) and comparing the infill ($\Delta E-2$). For each sample, measurements were taken at different points of the dough, crust, and crumb to ensure representative color evaluation.

2.6.3. Porosity analysis of crumb

Digital pictures were taken from horizontal cross-sectional slices of 20 mm thickness, obtained by cutting each bread sample through its central region. The image of the center of each slice was cropped to a square of 2.6 × 2.6 cm², which was defined as the Region of Interest (ROI) for analysis. The image was binarized using the **Modified IsoData automatic thresholding algorithm** to allow the conversion into black and white. Black dots represent porous. After this processing, the number of pores, the pores total area (cm²), pores average area (cm²), and the porosity (%) were determined. Images were analyzed using ImageJ Software (NIH, Washington, DC, USA)

2.7. Statistical analysis

Two-way ANOVA and post-hoc Fisher's least significant differences (LSD) were applied to establish significant statistical differences between samples. All statistical analyses were performed with the XLSTAT 2024.3.0 software (Lumivero, 2023) and differences were considered significant at $p < 0.05$.

3. Results and discussion

3.1. Rheological and colorimetric properties of gluten-free bread doughs

It is essential to understand the rheological properties of the gluten-free dough to know its printability before the 3D printing process (Maldonado-Rosas et al., 2022). The results of the rheological analysis showed that the dough presented a predominantly elastic behavior, with an elastic modulus (G') of 2068 ± 227 Pa higher than the viscous modulus (G'') of 419 ± 42 Pa. This characteristic was confirmed by the $\tan \delta$ value (0.203 ± 0.002), indicating a solid behavior with a complex modulus (G^*) of 2110 ± 231 Pa and a complex viscosity (η^*) of 335 ± 36 Pa•s.

The colorimetric analysis of the dough showed values of $L^* = 82.47 \pm 2.07$, indicating a luminous sample, with chromatic coordinates $a^* = -0.99 \pm 0.05$ and $b^* = 6.66 \pm 1.12$. The C^* was 6.74 ± 1.12 and the h^* was 98.6 ± 1.3 , corresponding to an achromatically white sample, characteristic of bread doughs.

These results are consistent with other studies on 3D printing of gluten-free doughs. Matas et al. (2022), printing gluten-free doughs with rosehip, reported a predominantly elastic behavior in their control sample, with comparable rheological and colorimetric values. Similar findings were reported by Lazaridou et al. (2007) and Yazar & Demirkesen (2023) in gluten-free doughs with different hydrocolloids, where they observed that the elastic modulus dominated over the viscous modulus, indicating a predominantly elastic behavior.

3.2. Determination of printed sample weight and moisture loss after baking

Fig. 2 shows the weight of the printed samples (a) and the percentage of moisture loss after baking (b) for the different patterns (rectilinear and concentric) and infill percentages (30 %, 40 %, 50 %, and 60 %). Statistical analysis revealed a significant interaction ($p < 0.05$) between pattern and infill percentage for printed weight. As seen in **Fig. 2a**, samples with concentric patterns presented lower weight than samples with rectilinear patterns for all infill percentages. In addition, an increasing trend in weight was observed as the infill percentage increased for both patterns, with significant differences ($p < 0.05$) between all samples except for R40 and C60. This is due to a higher percentage of infill requires a greater amount of material to occupy the same volume. The weight difference between patterns should be considered during the design and production of 3D-printed food, especially when precise control is required or when there are weight restrictions in the final applications. The difference in weight between the two patterns could be attributed to the way the material is deposited and distributed within the structure, where the rectilinear pattern causes a higher material accumulation. Rectilinear pattern generates a higher number of trajectories per layer due to the way it covers the area by alternating lines. This implies a greater amount of deposited mass per layer compared to the concentric pattern. As expected, it was also observed that the weight of all samples decreased after baking, which was due to the fact that the moisture in the samples evaporated quickly after exposure to hot air, leading to a decrease in the final weight (Lv et al., 2024).

Regarding moisture loss (**Fig. 2b**), the statistical analysis showed no significant interaction ($p > 0.05$) between pattern and infill percentage, indicating that the effect of infill percentage on moisture loss is independent of the pattern used. It was observed that samples with a lower percentage of infill (30 %) presented higher moisture losses during baking in both patterns, with a decreasing trend as the percentage of infill increased. This phenomenon could be explained by the fact that the structure with a lower percentage of infill facilitates the diffusion and evaporation of water during the baking process. Structures with a higher percentage of infill present a denser network that could hinder the escape of moisture, resulting in lower weight losses.

3.3. Dimensional changes after the printing and baking process

Dimensional changes during printing and post-processing are a critical factor in food 3D printing, as they directly affect the accuracy and quality of the final product. **Table 1** shows the top and front views of 3D printed and baked bread samples with different patterns (concentric and rectilinear) and infill percentages (30 %, 40 %, 50 %, and 60 %). According to visual perception, morphological differences were observed depending on both the pattern and the infill percentage. Samples printed with a rectilinear pattern showed a rectangular structure and remained uniform. However, after baking, a loss of pattern definition and an increase in volume, especially in width, was observed, as shown in the top views. On the other hand, the printed samples with concentric patterns showed less structural stability. After the baking process, the expansion is mainly in height (Zhang et al., 2022).

The deviations (%) in height, width, and length of the printed (a) and baked (b) samples are shown in **Fig. 3**. During printing (**Fig. 3a**), significant differences ($p < 0.05$) were observed in the deviations of the dimensions according to pattern and infill. LSD analysis revealed significant differences ($p < 0.05$) in height deviation between concentric and rectilinear patterns for 30 %, 40 %, and 50 % infill. The rectilinear pattern showed greater deviations, possibly because some of the infill lines were deposited very close to the outer walls of the structure. This led to partial fusion between the infill and the walls, resulting in a localized accumulation of mass in those areas. This effect can be visually observed in the top view images presented in **Table 1**. In addition, the rectilinear pattern exhibited greater structural stability. The straight lines arranged in alternating directions formed a more robust internal framework. In contrast, the concentric pattern, composed of less interconnected circular paths, showed lower structural rigidity and tended to collapse slightly, which limited vertical expansion and reduced height deviations. Both rectilinear and concentric patterns showed a tendency for height deviations to increase as the percentage of infill increased from 30 % to 50 %. However, at 60 % infill, the height deviations decreased slightly compared to 50 %. This behaviour can be attributed to the increase in weight at higher infill densities, which could cause compression of the printed layers, limiting the height expansion. For 60 % infill, no significant differences ($p > 0.05$) were found between patterns. In terms of width, the concentric pattern showed significantly ($p < 0.05$) larger deviations than the rectilinear pattern for all percentages

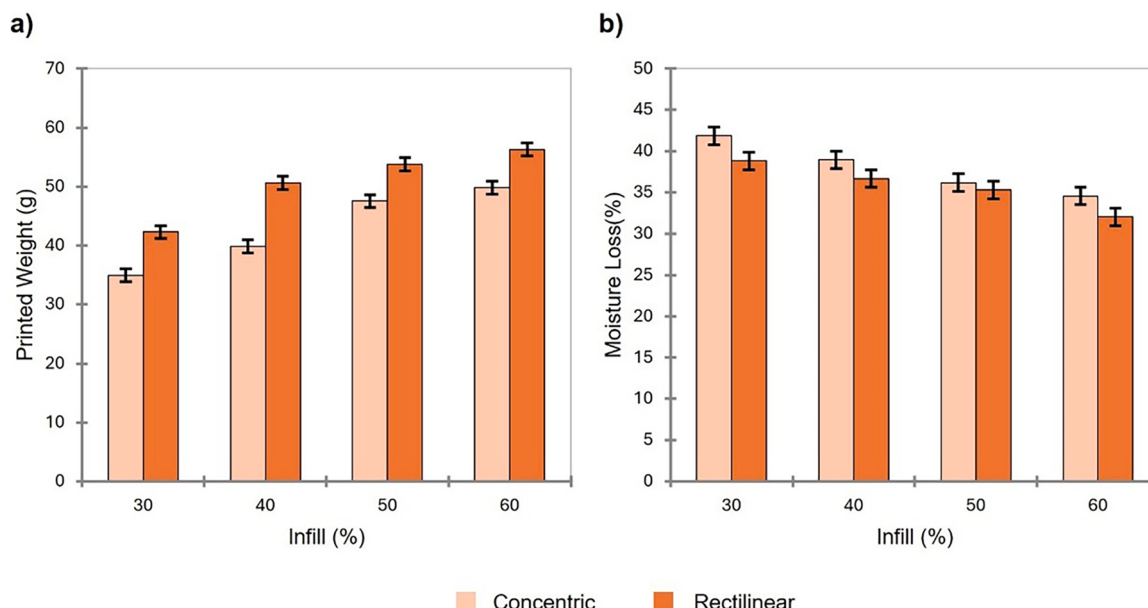


Fig. 2. a) Printed sample weight (g) and b) Moisture loss (%) after baking for concentric and rectilinear patterns with different infill percentages (30 %, 40 %, 50 %, and 60 %). Error bars represent the least significant difference (LSD) at $p < 0.05$ significance level.

Table 1

3D printed samples before and after baking according to the filling pattern (rectilinear and concentric) and infill percentage (30 %, 40 %, 50 %, and 60 %), showing top and front views.

Infill (%)	View	Pattern			
		Rectilinear		Concentric	
		Printing	Baking	Printing	Baking
30	Top				
	Front				
40	Top				
	Front				
50	Top				
	Front				
60	Top				
	Front				

2

except for 30 % infill, with a decreasing trend as the infill percentage increased. This larger deviation in the concentric pattern can be attributed to its structure of continuous circles without intersections, which provides less structural stability and allows for greater lateral deformation during printing. The rectilinear pattern showed no significant differences ($p > 0.05$) among samples with 40 %, 50 %, and 60 % infill, suggesting that its rectilinear structure provides greater resistance to deformation in width. The deviations in length, although relatively smaller compared to the other dimensions, showed significant differences ($p < 0.05$) between patterns for all infill percentages, registering negative values for the concentric pattern with 30 % infill and no significant differences ($p > 0.05$) found between the 40 %, 50 %, and 60 % infill levels. For the rectilinear pattern, the same trend observed in the height dimension was noted as the infill percentage increased; the length deviations also increased, but at 60 % infill, the deviation in length was considerably lower. This may be due to the fact that at 60 % infill, the internal structure becomes denser and more rigid, and the greater structural weight results in more uniform compression, reducing deviations as the layers settle on a more solid base. This phenomenon was also investigated by Liu, Bhandari, et al. (2018) in their study on 3D printing of mashed potato, where they observed that infill levels below 40 % led to partial structural collapse, while higher levels formed a more stable structure that prevented deformation.

The printed samples showed these dimensional variations with

respect to the target figure, also because of the fermentation process. The fermentative process, due to the yeast and the viscoelastic behaviour of the bread dough, causes a swelling of the matrix. As observed by Al-Muslimawi et al. (2013), viscoelastic fluids tend to expand to a diameter larger than that of the nozzle due to the release of the force exerted by the tip walls on the fluids.

During baking (Fig. 3b), the height deviations showed significant differences ($p < 0.05$) between patterns with 50 % and 60 % infill, where the concentric pattern showed an increasing trend. For 30 % and 40 % infill, the differences in height were not statistically significant ($p > 0.05$). Significant ($p < 0.05$) differences were more pronounced for width, especially with 50 % infill, where the rectilinear pattern showed a significantly greater expansion than the concentric pattern. Regarding length, all samples experienced shrinkage during baking, with significant differences between patterns mainly at 50 % and 60 % infill, being more pronounced in the concentric pattern with 60 % infill. The overall shrinkage was due to moisture loss during baking.

Matas et al. (2022) studied the 3D printing of gluten-free breads with different heights using a rectilinear pattern with 60 % infill. Their results showed a deformation of the bread after baking, predominantly in height, as they made a small incision in the surface so that the CO₂ produced during baking diffused there and not laterally. This contrasts with the results of this experience. In this case, the absence of incisions, CO₂ expansion occurs both vertically and laterally, and this process was

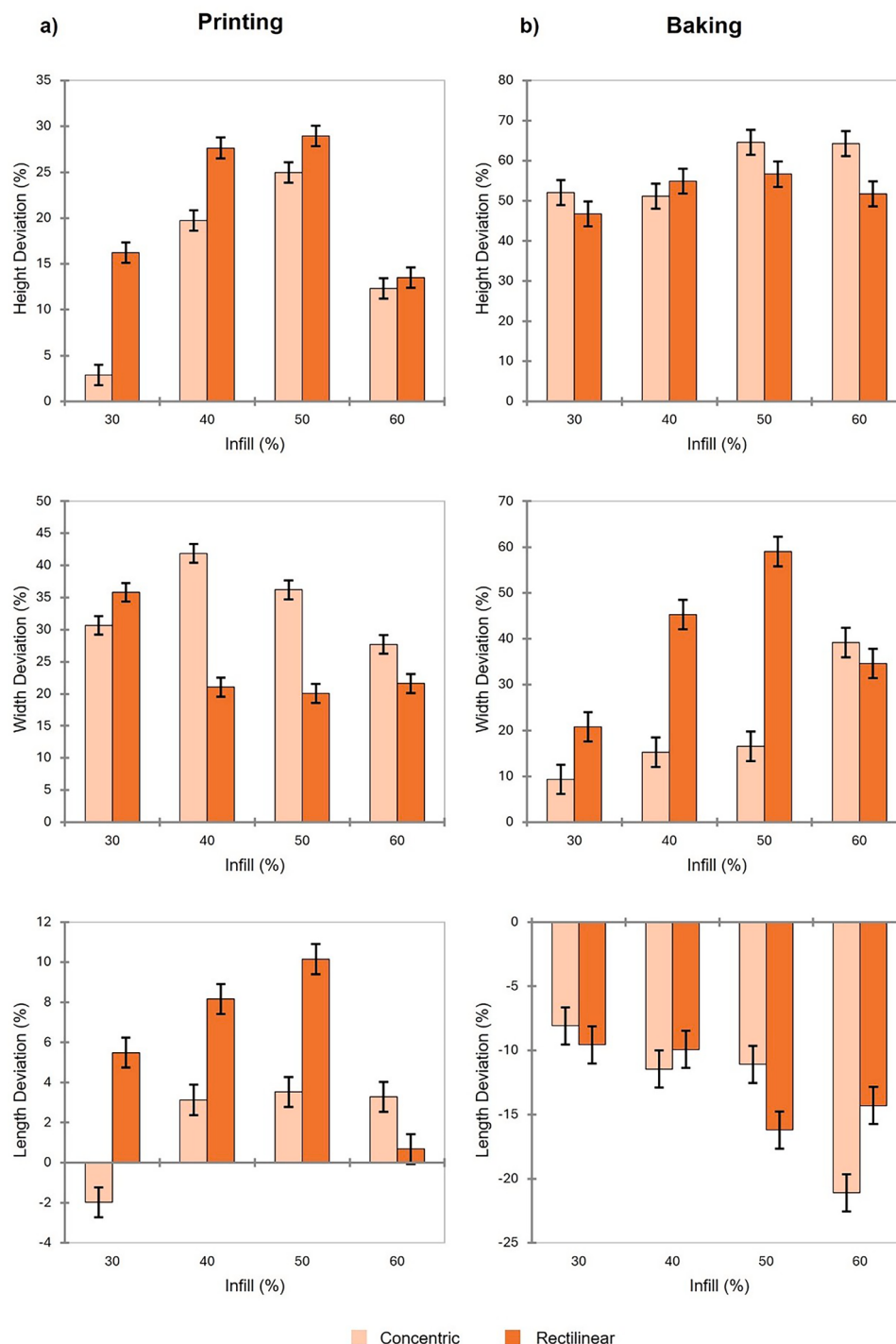


Fig. 3. Dimensional deviations in 3D-printed gluten-free bread using different patterns and infill. (a) Deviations after printing and (b) Deviations after baking, showing height, width, and length variations for concentric and rectilinear at 30 %, 40 %, 50 %, and 60 % infill densities. Error bars represent the least significant difference (LSD) at $p < 0.05$ significance level.

influenced by the type of filler pattern used. As shown in Table 1, the concentric pattern, by creating continuous circular layers without intersections, resulted in greater moisture loss and allowed a more pronounced expansion in height during baking, especially at high infill percentages. This more open structure of the concentric pattern allowed the steam generated during baking to escape more easily in the vertical direction. In contrast, the rectilinear pattern, which creates a network of perpendicular intersections, showed a more limited vertical expansion, possibly because this more reticulated structure restricts expansion in

height and diverts the steam pressure generated towards lateral expansion. Therefore, samples with a rectilinear pattern showed greater deviations in width, especially with high percentages of infill, where the network of intersections is denser and further hinders vertical expansion and moisture loss in that direction.

3.4. Post-baking color

Crust and crumb color during the baking process can be indicative of

bread quality and consumer preferences (Torres-Pérez et al., 2024). Crust browning and crumb color are a direct consequence of thermal processes occurring during baking, such as the Maillard reaction and caramelization (Naqash et al., 2017). These processes are strongly influenced by the internal structure of the bread, which depends on the pattern and percentage of filler used in 3D printing. Differences in structural density affect heat dissipation, moisture retention and, consequently, color development (Mudau and Adebo, 2024). The crust and crumb color changes of 3D-printed bread with different patterns and infills are shown in Table 2. In the crust observed that the lightness (L^*) reached maximum values with 60 % infill in both patterns, being significantly different ($p < 0.05$) with respect to the other infill percentages. The concentric pattern showed a progressive increase in lightness with increasing infill percentage. The values of a^* were generally low in all the samples, indicating a slight tendency towards red, with the rectilinear sample with 60 % infill showing the highest value, with significant differences ($p < 0.05$) with respect to the concentric sample with 60 % infill. As for the b^* parameter, the highest values were observed in the intermediate infills (40 % and 50 %) for both patterns, with significant differences ($p < 0.05$) with respect to the 30 % and 60 % infill. Samples with 60 % infill had the lowest b^* values, with no significant differences between plots ($p > 0.05$).

Regarding the crumb, it was observed that as the percentage of infill increased, the brightness value (L^*) increased in both patterns, with a more pronounced increase in the rectilinear pattern. The a^* values were low, reaching their maximum in the samples with 30 % infill for both patterns with no significant differences between them ($p > 0.05$). The b^* parameter showed different behaviors depending on the pattern: in the rectilinear pattern, a gradual decrease was observed with increasing infill, while in the concentric pattern, the minimum values occurred at intermediate infills of 40 % and 50 %, without following a gradual pattern.

The color differences between patterns ($\Delta E-1$) for both crust and crumb were very similar, being more pronounced with 60 % infill in both cases. The differences between infills ($\Delta E-2$) are greater in the samples with rectilinear patterns for both crust and crumb. Therefore, color differences were observed as they were higher than 3 units (the limit perceptible by humans) (Igual et al., 2021). These results indicate that changes in infill percentage produce more marked color differences than pattern-type changes in crust and crumb. This effect can be attributed to differences in heat and moisture dynamics during baking. As shown in Fig. 2b, samples with higher infill percentages exhibited lower moisture loss, particularly those with rectilinear patterns. This greater water retention likely delayed surface dehydration, reducing Maillard browning at early baking stages. However, the denser and more compact structure of the rectilinear pattern may have restricted steam

release, leading to localized heat buildup (Dessev et al., 2020). Once the surface moisture evaporated, these areas could have browned more rapidly and intensely, contributing to the higher a^* values and more pronounced color differences observed.

3.5. Crumb image analysis

Bread crumb structure provides an accurate quantitative description of crumb characteristics in terms of pores density, total pore area, average pore size, and total porosity. Therefore, structure characterization plays an essential role in the mechanical properties of bread and the development of products with the desired quality. To evaluate bread crumb structure, image analysis is a convenient and useful tool to qualify and quantify the characteristics of crumb structure (Falcone et al., 2004; Rathnayake et al., 2018). Table 3 shows the porous crumb structure of the 3D-printed gluten-free breads visualized by grey-scale images and corresponding binarization. Table 4 shows the quantitative analysis of the crumb-porous structure. Crumb porosity was expressed as the mean value of the total pore/total area ratio in each slice of the considered volume (Rathnayake et al., 2018). The results revealed that samples with concentric patterns showed higher total porosity, with values ranging between 18 % and 28 %, while samples with rectilinear patterns presented porosity values between 14 % and 24 %, finding only significant differences ($p < 0.05$) between R60 and C30. A higher porosity suggests an increase in the number of larger pores and, consequently a decrease in the degree of porous uniformity (Rathnayake et al., 2018).

Pore density (pores/cm²) showed a variable trend according to the percentage of infill. In the rectilinear pattern, the highest density was observed with 40 % infill (12 pores/cm²), followed by 50 % (10 pores/cm²) with no significant differences ($p > 0.05$), which is reflected in the binary images in Table 3 as a more uniform and regular distribution of small pores. For the concentric pattern, samples C30-C50 maintained a relatively constant pore density (8–11 pores/cm²), while sample C60 showed a significant reduction to 1.9 pores/cm². This fact is clearly visible in the image of sample C60, where larger but less numerous pores are visible, compensating for the low pore density with a significantly larger average pore size (0.12 cm²), resulting in a total porosity of 23 %.

The total porous area was consistently larger in the concentric samples, reaching a maximum of 2.13 cm² in sample C60, while in the rectilinear samples, it did not exceed 1.4 cm². Table 3 shows that the concentric pattern had a more irregular distribution of pores and more extensive porous areas. This structure suggests that the concentric printing pattern promotes the formation of a more open structure in the bread crumb, possibly due to the concentric arrangement of the weft that could allow a greater expansion of the dough during baking.

Table 2

Mean values and standard deviations of color parameters L^* , a^* , b^* , C^* , h^* and color differences ($\Delta E-1$ and $\Delta E-2$) of crust and crumb of gluten-free bread.

	Pattern	Infill	L^*	a^*	b^*	C^*	h^*	$\Delta E-1$	$\Delta E-2$
Crust	Rectilinear	30	66.5 (1.8) ^{bc}	1.3 (0.2) ^b	20.1 (0.3) ^{cd}	20.1 (0.3) ^{cd}	86.3 (0.7) ^{bc}	3.2 (1.5) ^b	–
	Rectilinear	40	61.9 (1.3) ^e	1.4 (0.5) ^b	30.2 (0.9) ^a	30.2 (0.9) ^a	87.3 (0.8) ^b	2.8 (0.7) ^b	11.1 (1.2) ^a
	Rectilinear	50	62.7 (1.6) ^{de}	1.35 (1.07) ^b	30.1 (0.5) ^a	30.1 (0.6) ^a	87 (2) ^b	4.1 (0.4) ^{ab}	10.742 (1.108) ^a
	Rectilinear	60	68.4 (1.5) ^{ab}	4.2 (0.8) ^a	19.4 (0.5) ^{de}	19.9 (0.6) ^d	77.8 (1.9) ^d	5.5 (0.3) ^a	3.8 (0.5) ^b
	Concentric	30	63.7 (1.3) ^{de}	2.1 (0.5) ^b	21.5 (0.9) ^c	21.6 (0.9) ^c	84.7 (1.3) ^c	–	–
	Concentric	40	61.4 (1.3) ^e	1.42 (0.95) ^b	27.7 (0.6) ^b	27.8 (0.6) ^b	87.1 (1.9) ^{bc}	–	6.9 (0.5) ^{ab}
	Concentric	50	64.7 (0.6) ^{cd}	1.3 (0.6) ^b	26.6 (0.2) ^b	26.7 (0.2) ^b	87.2 (1.3) ^{bc}	–	5.35 (0.17) ^b
	Concentric	60	70.5 (1.2) ^a	-0.3 (0.4) ^c	17.9 (1.9) ^e	17.9 (1.9) ^e	91.02 (1.12) ^a	–	8.1 (1.4) ^a
Crumb	Rectilinear	30	75.37 (1.13) ^d	1.96 (1.16) ^{ab}	18.5 (1.9) ^{ab}	18.6 (1.9) ^{ab}	84 (4) ^{cd}	2.3 (0.5) ^c	–
	Rectilinear	40	82.6 (0.4) ^b	-2.04 (1.04) ^{cd}	18.77 (0.12) ^a	18.9 (0.2) ^{ab}	96 (3) ^b	5.3 (1.2) ^b	8.3(0.8) ^b
	Rectilinear	50	82 (2) ^b	-2.8 (0.8) ^{cd}	17.3 (1.7) ^{ab}	17.6 (1.7) ^{ab}	99(3) ^{ab}	3.2 (0.9) ^c	8.1 (1.9) ^b
	Rectilinear	60	87.2 (0.9) ^a	0.8 (1.5) ^b	16.81 (1.06) ^{ab}	16.87 (1.08) ^{ab}	88(5) ^c	7.1 (0.2) ^a	12.1 (1.2) ^a
	Concentric	30	75.7 (1.8) ^{cd}	3.3 (0.8) ^a	18.3 (1.2) ^{ab}	18.6 (1.2) ^{ab}	80 (2) ^d	–	–
	Concentric	40	77.9 (0.8) ^c	-1.5 (0.5) ^c	17 (2) ^{ab}	17 (2) ^{ab}	94.8 (1.5) ^b	–	5.7 (0.7) ^b
	Concentric	50	82 (3) ^b	-3.4 (0.7) ^d	16 (2) ^b	16 (2) ^b	101.95 (1.05) ^a	–	9.8(1.6) ^a
	Concentric	60	80.8 (0.5) ^b	1.4 (0.9) ^b	19.3 (0.8) ^a	19.4 (0.8) ^a	86 (3) ^c	–	5.6 (0.3) ^b

The letters (a-d) in columns indicate the homogeneous groups according to ANOVA ($p < 0.05$), calculated separately for crust and crumb.

Table 3

Comparative analysis of the porous structure of 3D printed gluten-free bread with different infill percentages (30–60 %) and printing patterns (rectilinear and concentric) visualized by grayscale images and their corresponding binarization.

Infill	Pattern	
	Rectilinear	Concentric
30		
40		
50		
60		

Note: Porosity values were calculated by image analysis from representative 2D cross sections of the bread samples. The images were taken from the central region of each piece after its horizontal cut. The ROI selected for analysis was $2.6 \times 2.6 \text{ cm}^2$ in the central region of each section.

Table 4

Mean values and standard deviations of the porous structure in 3D printed gluten-free bread samples with different patterns and infills.

Sample	Porous/ cm ²	Total porous area (cm ²)	Average porous size (cm ²)	Porosity (%)
R30	5 (3) ^{cd}	0.9 (0.4) ^b	0.04 (0.03) ^b	18 (8) ^{ab}
R40	12 (4) ^a	1.3 (0.5) ^{ab}	0.022 (0.009) ^b	24 (7) ^{ab}
R50	10 (4) ^{ab}	1.4 (0.6) ^{ab}	0.021 (0.005) ^b	19 (9) ^{ab}
R60	7 (4) ^{bc}	0.8 (0.4) ^b	0.022 (0.007) ^b	14 (7) ^b
C30	8(2) ^{bc}	1.8 (0.5) ^{ab}	0.041 (0.015) ^b	28 (4) ^a
C40	11(2) ^{ab}	1.3 (0.6) ^{ab}	0.018 (0.003) ^b	20 (5) ^{ab}
C50	9(2) ^{abc}	1.4 (0.6) ^{ab}	0.022 (0.004) ^b	18 (5) ^{ab}
C60	1.9 (0.3) ^d	2.13 (1.13) ^a	0.12 (0.06) ^a	23 (7) ^{ab}

The letters (a-d) in columns indicate the homogeneous groups according to ANOVA ($p < 0.05$). (R: rectilinear; C: concentric).

Analysis of the pore size distribution (Fig. 4) provides additional information on the structural differences between the two printing patterns. For the rectilinear pattern (Fig. 4a), a pronounced peak of porosity is observed between 0.001–0.002 cm², where samples reached maximum values between 17–24 % porosity. Sample R30 showed the highest peak (23.83 %), while sample R60 presented the lowest peak (17.61 %). After 0.01 cm², all samples showed a significant decrease in porosity, with small fluctuations.

For the concentric pattern (Fig. 4b), the main porosity peak was also between 0.001–0.002 cm², with more uniform maximum values among the different samples (17–22 %). However, sample C60 presented a more differentiated distribution, with a wider peak and a more noticeable presence of large pores ($>0.1 \text{ cm}^2$) compared to the rectilinear pattern.

Comparing both patterns, the rectilinear pattern showed a more concentrated distribution around the main pore size, while the concentric pattern presented a more dispersed distribution with a greater presence of large pores, which corroborates the data on total pore area and mean pore size. The influence of the percentage of infill seems to be more pronounced in the rectilinear pattern, where clearer

differences were observed between the peaks of the different samples.

These results on pore structure were similar to those reported by Derossi et al. (2020), who found that the 3D printing process significantly affects the microstructure of the final product. In their study with cereal-based products, they observed that 3D printing generates larger pores, but in smaller numbers, similar to what was found in our samples with concentric patterns. In addition, they also observed that the position of the pores is strongly influenced by the printing movements, which is consistent with our observations on the more irregular pore distribution in the concentric pattern (Derossi et al., 2020).

These differences in pore structure could have significant implications on the quality of the final product. Higher porosity and pore size, as observed in concentric samples, is generally associated with lower compressive strength, resulting in lower hardness. This characteristic can negatively influence the quality of the crumb. On the other hand, the more uniform structure of the rectilinear pattern with smaller pores could be related to higher density and possibly higher hardness, characteristics that are important in the quality of the final product (Arendt et al., 2008; Puerta et al., 2020).

4. Conclusion

The design parameters of the internal structure, specifically the pattern and percentage of infill, significantly influence the dimensional stability, color characteristics, and crumb structure of the 3D-printed gluten-free bread. The rectilinear pattern showed greater dimensional stability during printing, particularly in width and length, while the concentric pattern showed greater variations in these dimensions. However, during baking, the behavior was reversed, with the concentric pattern showing greater stability and higher moisture losses, as its structure promoted steam escape and consequently reduced shape deviations. Colorimetric analysis revealed that both patterns and infill percentages significantly affected the final crust and crumb color, with differences being more pronounced in samples with higher infill percentages and more noticeable in samples with a rectilinear pattern. Analysis of crumb structure showed different characteristics between

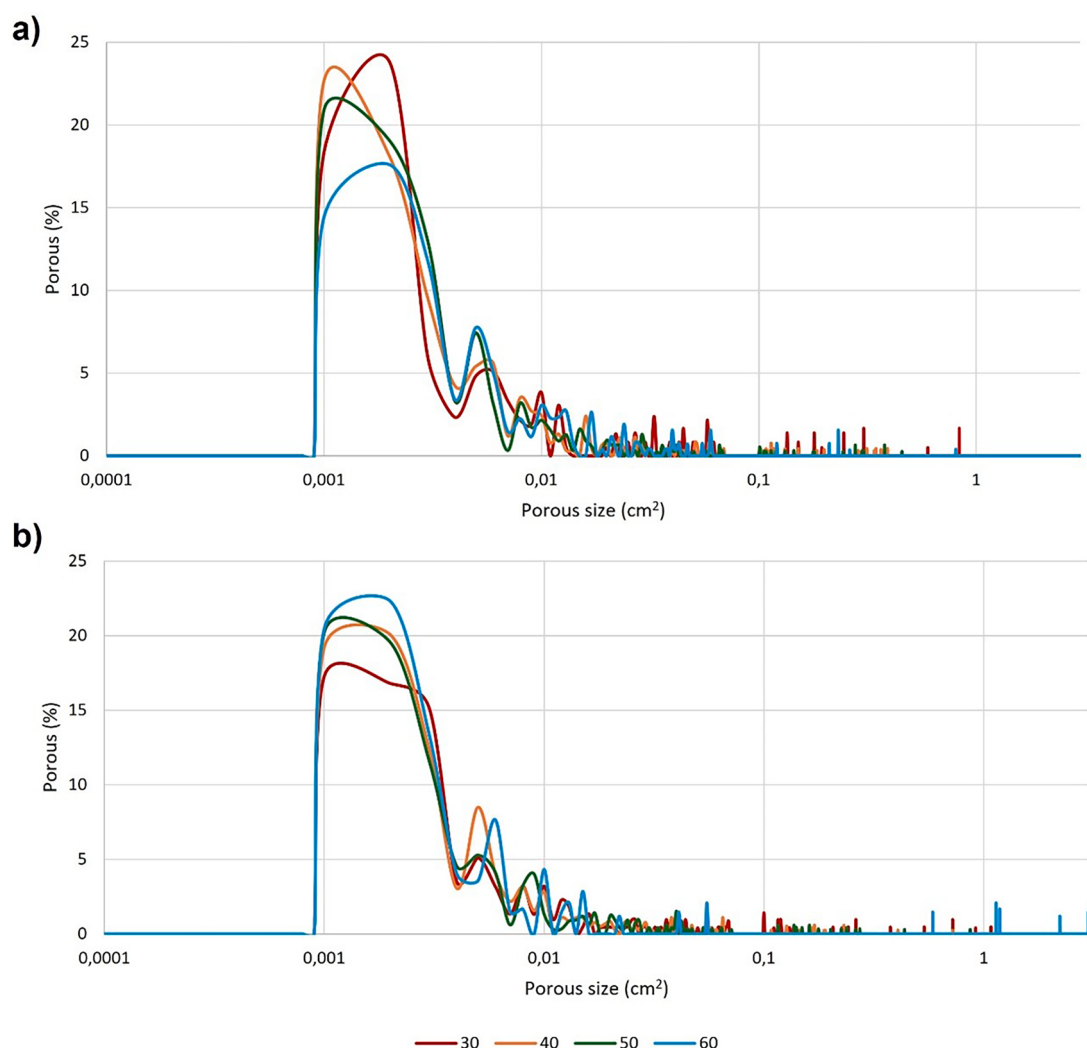


Fig. 4. Pore size distribution of 3D printed gluten-free bread with different infill percentages (30–60 %): a) rectilinear pattern and b) concentric pattern.

patterns, with the concentric pattern generally producing higher total porosity compared to the rectilinear pattern. The concentric pattern resulted in a more irregular distribution of pores with larger, but less numerous alveoli, particularly with 60 % infill, while the rectilinear pattern produced a more uniform distribution of smaller pores, especially with 40–50 % infill.

Considering that in bakery products, a uniform crumb structure is typically desired for consistent quality and texture, the rectilinear pattern with 40–50 % infill would be the most suitable option for 3D printed gluten-free bread, as it provides both dimensional stability during printing and a more uniform structure. The concentric pattern, while producing higher total porosity and fewer dimensional deviations after baking, results in a less uniform crumb structure that deviates from traditional bakery quality standards. This understanding of the relationship between internal structure design parameters and final product characteristics provides the foundation for future optimization of 3D-printed gluten-free bread products to meet specific product quality requirements.

Funding

This research was funded by Conselleria de Innovación, Universidades, Ciencia y Sociedad Digital, Generalitat Valenciana, grant number CIAICO/2023/173, and from MCIN/AEI/10.13039/501100011033/ through project PID2020-115973RB-C22 and the FPI

PhD contract granted by the Universitat Politècnica de Valencia subprograma 1 (PAID 01 21).

Ethical statement

Do not apply for this work, as it does not involve research on humans or animals.

CRediT authorship contribution statement

Carmen Molina-Montero: Methodology, Formal analysis, Conceptualization, Writing – original draft, Investigation, Data curation. **Adrian Matas:** Investigation, Conceptualization, Methodology, Formal analysis. **Marta Igual:** Writing – review & editing, Investigation, Conceptualization, Methodology, Formal analysis. **Javier Martínez-Monzó:** Writing – review & editing, Resources, Conceptualization, Supervision, Funding acquisition. **Purificación García-Segovia:** Supervision, Funding acquisition, Writing – review & editing, Project administration, Conceptualization.

Declaration of competing interest

The authors declare that they have no known competing financial interests or personal relationships that could have appeared to influence the work reported in this paper.

Acknowledgments

The authors want to acknowledge Sinblat Alimentación Saludable S.L. providing gluten-free mix used for experiments and the FPI PhD contract granted by the Universitat Politècnica de València subprograma 1 (PAID 01 21).

Data availability

Data will be made available on request.

References

- Al-Muslimawi, A., Tamaddon-Jahromi, H.R., Webster, M.F., 2013. Simulation of viscoelastic and viscoelastoplastic die-swell flows. *J. Nonnewt. Fluid Mech.* 191, 45–56. <https://doi.org/10.1016/j.jnfm.2012.08.004>.
- Arendt, E.K., Morrissey, A., Moore, M.M., Dal Bello, F., 2008. *Gluten-free breads. Gluten-Free Cereal Products and Beverages*. Academic Press, pp. 289–319.
- Bulut, E.G., Candogam, K., 2022. Development and characterization of a 3D printed functional chicken meat based snack: optimization of process parameters and gelatin level. *Lwt* 154 (November 2021). <https://doi.org/10.1016/j.lwt.2021.112768>.
- Caporizzi, R., Derossi, A., Severini, C., 2018. Cereal-based and insect-enriched printable food: from formulation to postprocessing treatments. Status and perspectives. *Fundam. 3D Food Print. Appl.* <https://doi.org/10.1016/B978-0-12-814564-7.00004-3>. Elsevier Inc.
- Chen, X.huan, Zhang, M., Teng, X.xiu, Mujumdar, A.S., 2022. Internal structure design for improved shape fidelity and crispness of 3D printed pumpkin-based snacks after freeze-drying. *Food Res. Int.* 157 (March), 111220. <https://doi.org/10.1016/j.foodres.2022.111220>.
- Decante, G., Costa, J.B., Silva-Correia, J., Collins, M.N., Reis, R.L., Oliveira, J.M., 2021. Engineering bioinks for 3D bioprinting. *Biofabrication* 13 (3). <https://doi.org/10.1088/1758-5090/abec2>. IOP Publishing Ltd.
- Demei, K., Zhang, M., Phuhongsung, P., Mujumdar, A.S., 2022. 3D food printing: controlling characteristics and improving technological effect during food processing. *Food Res. Int.* 156 (March). <https://doi.org/10.1016/j.foodres.2022.111120>.
- Derossi, A., Caporizzi, R., Azzollini, D., Severini, C., 2018. Application of 3D printing for customized food. A case on the development of a fruit-based snack for children. *J. Food Eng.* 220, 65–75. <https://doi.org/10.1016/j.jfoodeng.2017.05.015>.
- Derossi, A., Caporizzi, R., Oral, M.O., Severini, C., 2020. Analyzing the effects of 3D printing process per se on the microstructure and mechanical properties of cereal food products. *Innov. Food Sci. Emerg. Technol.* 66 (October), 102531. <https://doi.org/10.1016/j.ifset.2020.102531>.
- Dessev, T., Lalanne, V., Keramat, J., Jury, V., Prost, C., Le-Bail, A., 2020. Influence of baking conditions on bread characteristics and acrylamide concentration. *J. Food Sci. Nutr. Res.* 03 (04). <https://doi.org/10.26502/jfsnr.2642-11000056>.
- Falcone, P.M., Baiano, A., Zanini, F., Mancini, L., Tromba, G., Montanari, F., Del Nobile, M.A., 2004. A novel approach to the study of bread porous structure: phase-contrast X-ray microtomography. *J. Food Sci.* 69 (1). <https://doi.org/10.1111/j.1365-2621.2004.tb17865.x>.
- Feng, C., Zhang, M., Bhandari, B., 2019. Materials properties of printable edible inks and printing parameters optimization during 3D printing: a review. *Crit. Rev. Food Sci. Nutr.* 59 (19), 3074–3081. <https://doi.org/10.1080/10408398.2018.1481823>.
- Fernandez-Vicente, M., Calle, W., Ferrandiz, S., Conejero, A., 2016. Effect of infill parameters on tensile mechanical behavior in desktop 3D printing. *3D Print. Addit. Manuf.* 3 (3), 183–192. <https://doi.org/10.1089/3dp.2015.0036>.
- Godoi, F.C., Prakash, S., Bhandari, B.R., 2016. 3d printing technologies applied for food design: status and prospects. *J Food Eng* 179, 44–54. <https://doi.org/10.1016/j.jfoodeng.2016.01.025>. Elsevier Ltd.
- Igual, M., García-Segovia, P., Martínez-Monzo, J., 2021. Resistant maltodextrin's effect on the physicochemical and structure properties of spray dried orange juice powders. *Eur. Food Res. Technol.* 247 (5), 1125–1132. <https://doi.org/10.1007/s00217-021-03693-2>.
- Kim, H.W., Lee, J.H., Park, S.M., Lee, M.H., Lee, I.W., Doh, H.S., Park, H.J., 2018a. Effect of hydrocolloids on rheological properties and printability of vegetable inks for 3D food printing. *J. Food Sci.* 83 (12), 2923–2932. <https://doi.org/10.1111/1750-3841.14391>.
- Kim, H.W., Lee, J.H., Park, S.M., Lee, M.H., Lee, I.W., Doh, H.S., Park, H.J., 2018b. Effect of hydrocolloids on rheological properties and printability of vegetable inks for 3D food printing. *J. Food Sci.* 83 (12), 2923–2932. <https://doi.org/10.1111/1750-3841.14391>.
- Lazaridou, A., Duta, D., Papageorgiou, M., Belc, N., Biliaderis, C.G., 2007. Effects of hydrocolloids on dough rheology and bread quality parameters in gluten-free formulations. *J. Food Eng.* 79 (3), 1033–1047. <https://doi.org/10.1016/j.jfoodeng.2006.03.032>.
- Lille, M., Nurmelä, A., Nordlund, E., Metsä-Kortelainen, S., Sozer, N., 2018. Applicability of protein and fiber-rich food materials in extrusion-based 3D printing. *J. Food Eng.* 220, 20–27. <https://doi.org/10.1016/j.jfoodeng.2017.04.034>.
- Lin, Y.J., Punpongpanon, P., Wen, X., Iwai, D., Sato, K., Obrist, M., Mueller, S., 2020. FoodFab: creating food perception illusions using food 3D printing. In: Conference on Human Factors in Computing Systems - Proceedings. <https://doi.org/10.1145/3313831.3376421>.
- Lisovska, T., Harasym, J., 2023. 3D Printing progress in gluten-free food—Clustering analysis of advantages and obstacles. *Appl. Sci.* 13 (22), 12362. <https://doi.org/10.3390/app132212362>.
- Liu, Z., Bhandari, B., Prakash, S., Zhang, M., 2018a. Creation of internal structure of mashed potato construct by 3D printing and its textural properties. *Food Res. Int.* 111, 534–543. <https://doi.org/10.1016/j.foodres.2018.05.075>.
- Liu, Z., Zhang, M., 2021. Texture properties of microwave post-processed 3D printed potato snack with different ingredients and infill structure. *Future Foods*. 3. <https://doi.org/10.1016/j.fufo.2021.100017>.
- Liu, Z., Zhang, M., Bhandari, B., 2018b. Effect of gums on the rheological, microstructural and extrusion printing characteristics of mashed potatoes. *Int. J. Biol. Macromol.* 117, 1179–1187. <https://doi.org/10.1016/j.ijbiomac.2018.06.048>.
- Lumivero, 2023. XLSTAT statistical and Data Analysis Solution. Version 2023.1.4. Available at: <https://www.xlstat.com>.
- Lv, S., Li, H., Liu, Z., Cao, S., Yao, L., Zhu, Z., Hu, L., Xu, D., Mo, H., 2024. Preparation of Pleurotus eryngii protein baked food by 3D printing. *J. Food Eng.* 365. <https://doi.org/10.1016/j.jfoodeng.2023.111845>.
- Ma, Y., Zhang, L., 2022. Formulated food inks for extrusion-based 3D printing of personalized foods: a mini review. *Curr. Opin. Food Sci.* 44. <https://doi.org/10.1016/j.cofs.2021.12.012>. Elsevier Ltd.
- Maldonado-Rosas, R., Tejada-Ortigoza, V., Cuan-Urquiza, E., Mendoza-Cachú, D., Morales-de la Peña, M., Alvarado-Orozco, J.M., Campanella, O.H., 2022. Evaluation of rheology and printability of 3D printing nutritious food with complex formulations. *Addit. Manuf.* 58 (March). <https://doi.org/10.1016/j.addma.2022.103030>.
- Mancebo, C.M., San Miguel, M.Á., Martínez, M.M., Gómez, M., 2015. Optimisation of rheological properties of gluten-free doughs with HPMC, psyllium and different levels of water. *J. Cereal Sci.* 61, 8–15. <https://doi.org/10.1016/j.jcs.2014.10.005>.
- Manik, L.C.M., Nur, M., 2021. The recent development of gluten-free bread quality using hydrocolloids. *IOP Conf. Ser.: Earth Environ. Sci.* 733 (1). <https://doi.org/10.1088/1755-1315/733/1/012101>.
- Mantihal, S., Kobun, R., Lee, B.B., 2020. 3D food printing of as the new way of preparing food: a review. *Int. J. Gastron. Food Sci.* 22. <https://doi.org/10.1016/j.ijgfs.2020.100260>. AZTI-Tecnalia.
- Matas, A., Igual, M., García-Segovia, P., Martínez-Monzo, J., 2022. Application of 3D printing in the design of functional gluten-free dough. *Foods* 11 (11). <https://doi.org/10.3390/foods1111555>.
- Molina-Montero, C., Matas, A., Igual, M., Martínez-Monzo, J., García-Segovia, P., 2023. Impact of apricot pulp concentration on cylindrical gel 3D printing. *Gels* 9 (3), 253. <https://doi.org/10.3390/gels9030253>.
- Mudau, M., Adebo, O.A., 2024. Three dimensional (3D)-printed foods: a review of recent advances in their ingredients, printing techniques, food printers, post-processing methods, consumer acceptance and safety. *J. Food Proc. Eng.* 47 (5). <https://doi.org/10.1111/jfpe.14621>. John Wiley and Sons Inc.
- Naqash, F., Gani, A., Gani, A., Masoodi, F.A., 2017. Gluten-free baking: Combating the challenges- A review. *Trends in Food Science & Technology* 66, 98–107. <https://doi.org/10.1016/j.tifs.2017.06.004>.
- Nijdam, J.J., LeCorre-Bordes, D., Delwart, A., Schon, B.S., 2021. A rheological test to assess the ability of food inks to form dimensionally stable 3D food structures. *J. Food Eng.* 291 (October 2019), 110235. <https://doi.org/10.1016/j.jfoodeng.2020.110235>.
- Pradhan, A., Saha, D., Tripathy, P.P., 2024. A multivariate study on the effect of 3D printing parameters on the printability of gluten-free composite dough. *J. Sci. Food Agric.* <https://doi.org/10.1002/jsfa.14031>.
- Puerta, P., Laguna, L., Villegas, B., Rizo, A., Fiszman, S., Tarrega, A., 2020. Oral processing and dynamics of texture perception in commercial gluten-free breads. *Food Res. Int.* 134. <https://doi.org/10.1016/j.foodres.2020.109233>.
- Pulatas, E., Su, J.W., Kenderes, S.M., Lin, J., Vardhanabhuti, B., Lin, M., 2022. Restructuring cookie dough with 3D printing: relationships between the mechanical properties, baking conditions, and structural changes. *J. Food Eng.* 319. <https://doi.org/10.1016/j.jfoodeng.2021.110911>.
- Rathanayake, H.A., Navaratne, S.B., Navaratne, C.M., 2018. Porous crumb structure of leavened baked products. *Int. J. Food Sci.* 2018. <https://doi.org/10.1155/2018/8187318>. Hindawi Limited.
- Severini, C., Derossi, A., Azzollini, D., 2016. Variables affecting the printability of foods: preliminary tests on cereal-based products. *Innov. Food Sci. Emerg. Technol.* 38, 281–291. <https://doi.org/10.1016/j.ifset.2016.10.001>.
- Sood, A.K., Ohdar, R.K., Mahapatra, S.S., 2010. Parametric appraisal of mechanical property of fused deposition modelling processed parts. *Mater. Des.* 31 (1), 287–295. <https://doi.org/10.1016/j.matdes.2009.06.016>.
- Tejada-Ortigoza, V., Cuan-Urquiza, E., 2022. Towards the development of 3D-printed food: a rheological and mechanical approach. *Foods* 11 (9). <https://doi.org/10.3390/foods11091191>.
- Torres-Pérez, R., Martínez-García, E., Siguero-Tudela, M.M., García-Segovia, P., Martínez-Monzo, J., Igual, M., 2024. Enhancing gluten-free bread production: impact of hydroxypropyl methylcellulose, psyllium husk fiber, and xanthan gum on dough characteristics and bread quality. *Foods* 13 (11). <https://doi.org/10.3390/foods13111691>.
- Voon, S.L., An, J., Wong, G., Zhang, Y., Chua, C.K., 2019. 3D food printing: a categorised review of inks and their development. *Virtual Phys. Prototyp.* 14 (3), 203–218. <https://doi.org/10.1080/17452759.2019.1603508>.
- Wang, X., Zhang, M., Phuhongsung, P., Mujumdar, A.S., 2024. Impact of internal structural design on quality and nutritional properties of 3D printed food products during post-printing: a critical review. *Crit. Rev. Food Sci. Nutr.* 64 (12), 3713–3724. <https://doi.org/10.1080/10408398.2022.2134979>. Taylor and Francis Ltd.

- Waseem, M., Tahir, A.U., Majeed, Y., 2024. Printing the future of food: the physics perspective on 3D food printing. *Food Phys.* 1, 100003. <https://doi.org/10.1016/j.foodp.2023.100003>.
- Yazar, G., Demirkesen, I., 2023. Linear and non-Linear rheological properties of gluten-free dough systems probed by fundamental methods. *Food Eng. Rev.* 15 (1), 56–85. <https://doi.org/10.1007/s12393-022-09321-3>. Springer.
- Zhang, L., Noort, M., van Bommel, K., 2022. Towards the creation of personalized bakery products using 3D food printing. *Adv. Food Nutr. Res.* 99, 1–35. <https://doi.org/10.1016/bs.afnr.2021.11.002>. Academic Press Inc.
- Zhao, L., Zhang, M., Chitrakar, B., Adhikari, B., 2021. Recent advances in functional 3D printing of foods: a review of functions of ingredients and internal structures. *Crit. Rev. Food Sci. Nutr.* 61 (21), 3489–3503. <https://doi.org/10.1080/10408398.2020.1799327>. Taylor and Francis Ltd.
- Zhu, S., Stieger, M.A., van der Goot, A.J., Schutyser, M.A.I., 2019. Extrusion-based 3D printing of food pastes: correlating rheological properties with printing behaviour. *Innov. Food Sci. Emerg. Technol.* 58 (July), 102214. <https://doi.org/10.1016/j.ifset.2019.102214>.